A Spectral Approach to Survival Probabilities in?Porous?Media

Journal of Statistical Physics
1

ISSN 0022-4715
Volume 141
Number 3

J Stat Phys (2010) 141:532-554
DOI 10.1007/
s10955-010-0054-1

Springer

J Stat Phys (2010) 141: 532–554
DOI 10.1007/s10955-010-0054-1

A Spectral Approach to Survival Probabilities in Porous Media

Binh T. Nguyen · Denis S. Grebenkov

Received: 3 May 2010 / Accepted: 26 August 2010 / Published online: 4 September 2010

Abstract We consider a diffusive process in a bounded domain with heterogeneously distributed traps, reactive regions or relaxing sinks. This is a mathematical model for chemical reactors with heterogeneous spatial distributions of catalytic germs, for biological cells with specific arrangements of organelles, and for mineral porous media with relaxing agents in NMR experiments. We propose a spectral approach for computing survival probabilities which are represented in the form of a spectral decomposition over the Laplace operator eigenfunctions. We illustrate the performances of the approach by considering diffusion inside the unit disk filled with reactive regions of various shapes and reactivities. The role of the spatial arrangement of these regions and its influence on the overall reaction rate are investigated in the long-time regime. When the reactivity is finite, a uniform filling of the disk is shown to provide the highest reaction rate. Although the heterogeneity tends to reduce the reaction rate, reactive regions can still be heterogeneously arranged to get nearly optimal performances.

Keywords Survival probability · Residence time · Heterogeneous media · Diffusion · Laplace operator

1 Introduction

Diffusion is a fundamental transport mechanism in physics, chemistry and biology [1–3]. During the diffusive exploration, particles may encounter traps, reactive regions or relaxing sinks which are distributed either in the bulk, or on the interface. While staying inside or in vicinity of these specific zones, particles may disappear with a given rate. This is a common mathematical model for many biological and industrial systems, e.g.

B.T. Nguyen · D.S. Grebenkov (✉)
Laboratoire de Physique de la Matière Condensée, CNRS – Ecole Polytechnique, 91128 Palaiseau, France
e-mail: denis.grebenkov@polytechnique.edu

B.T. Nguyen
e-mail: binh-thanh.nguyen@polytechnique.edu

1. chemical reactors with heterogeneous spatial distributions of catalytic germs [4, 5];
2. biological cells with specific arrangements of organelles [6, 7];
3. mineral porous media with relaxing agents in nuclear magnetic resonance (NMR) experiments [8].

If the system is isolated (no new particle is injected), the survival probability, as well as the concentration of the survived particles that diffuse in such a medium, decays in time. In the long-time regime, the survival probability exhibits an exponential decay, and the decay constant (i.e., the average "lifetime" of a diffusing particle) is expected to be proportional to the total amount, or "strength", of traps, relaxing sinks or reactive regions. This is a consequence of the classical Smoluchowski formula $\Phi \approx 4\pi D R c_0$ for the diffusive flux Φ of particles which are uniformly distributed with concentration c_0 and react on a single absorbing sphere of radius R, D being the diffusion coefficient of particles [9]. In particular, the diffusive flux is proportional to the size R of the sphere, not to its surface area $4\pi R^2$, as one could naively expect for reaction on a surface. For n well-separated absorbing spheres (a diluted suspension), the overall reaction rate k of a single diffusing particle is then $k \approx n\Phi/N \approx 3D\phi/R^2$, where $N = c_0 V$ is the number of diffusing particles and $\phi = n(4\pi R^3/3)/V$ is the volume fraction of absorbing spheres, V being the volume of the medium. It means that the overall reaction rate k (i.e., the decay constant) is proportional to the volume fraction ϕ of reactive grains (i.e., their total amount or "strength").

Since this seminal result, the survival probability of Brownian motion in reactive porous media was studied by different mathematical and numerical tools [1–3]. The asymptotic behavior of the survival probability in randomly located traps and the role of averaging over trap configurations were analyzed in a series of publications [10–13]. In the long-time limit, the survived particles reside in large voids, and the statistics of these voids leads to a stretched-exponential decay of the survival probability. Torquato and co-workers performed numerous Monte Carlo simulations in order to investigate how the reaction rate k depends on the volume fraction ϕ, the shape of individual reactive grains, their polydispersity, overlapping and reactivity, etc. [14–18]. Using the mean-field approximation, Richards proposed an explicit formula for the survival probability which was shown to be accurate for a wide range of times [19, 20]. Upper and lower bounds for the reaction rate were derived in a series of papers by Torquato and co-workers [21–25]. Riley et al. performed Monte Carlo simulations to study the dependence of the reaction rate on the reactivity and the spatial configuration of reactive grains [26]. Singer et al. dealt with the narrow escape problem to find an asymptotic expansion of the expected lifetime of Brownian motion as the absorbing part of the boundary shrinks to zero [27, 28]. Another insight onto this problem was brought by Bénichou and Voituriez [29]. The case of small traps was considered by Ward and co-workers who derived a number of rigorous asymptotic results [30–34]. A systematic perturbative approach was developed by Ryu et al. for studying the role of inhomogeneous spatial absorption [35, 36]. At last, the survival probability is closely related to first-passage and residence times whose properties have been actively studied during the last years [37–43].

Among various theoretical approaches for describing diffusive motion in confined domains, a spectral theory involving the Laplace operator eigenbasis provides perhaps the most fundamental insight onto this process. For instance, Brownstein and Tarr employed this description in order to explain multiexponential relaxation for water in biological cells [8]. During the past decade, several matrix formalisms were developed for both numerical and theoretical studies of restricted diffusion in NMR [44–49]. Recently, a matrix formalism was applied for computing the residence times and other functionals of reflected Brownian motion [50].

In a nutshell, the description starts from diffusion-reaction equation, in which traps, reactive regions or relaxing sinks are represented through a spatially heterogeneous trapping, reaction or relaxation rate $B(\mathbf{r})$. Following the ideas of a quantum mechanics perturbation theory, the reaction term is treated as a "perturbation" to the Laplace operator. The survival probability is then expressed in a matrix form involving two infinite-dimensional matrices: the diagonal matrix Λ representing the Laplace operator in its own basis, and a matrix $\mathcal{B}$ representing the reaction rate $B(\mathbf{r})$ in the Laplacian basis. Once these two matrices are computed, analytically or numerically, the survival probability takes an explicit multi-exponential form. Note that the survival probability can be seen as the cumulative distribution function of the survival time (i.e., the random moment at which reaction occurs or, equivalently, up to which the particle survives). The spectral approach thus provides a complete probabilistic description of the survival time, in sharp contrast to other theoretical approaches which were focused on the mean survival time.

The paper aims at revealing the role of a spatial heterogeneity $B(\mathbf{r})$ of traps, reactive regions or relaxing sinks onto the survival probability in the long-time regime. We study several model arrangements of reactive regions in order to increase the overall reaction performance of a medium, aiming in future at design of efficient catalysts or diffusive exchangers via optimization of their geometrical shapes. In other words, we address the question: for a fixed total amount or "strength" of reactive regions, what is the "optimal" shape and arrangement of these regions? Although the spectral approach is applicable to any bounded confining domain, we illustrate its concepts and performances by considering diffusion inside the unit disk which is filled with reactive grains. The explicit form of the Laplace operator eigenfunctions in the disk significantly simplifies computation and allows one to grasp the main features of the spectral approach. It is worth stressing that, in contrast to works by Ward and co-workers [30–34], our approach is not limited to small reactive regions and is in fact more accurate when these regions are extended. As a consequence, the spectral approach and perturbative techniques turn out to be complementary to each other.

The paper is organized as follows. In Sect. 2, we recall the derivation of a multi-exponential form of the survival probability. Section 3 summarizes the main steps for a numerical implementation of the spectral approach, error estimation and improvements. Numerical results, for both bulk and surface reactivity, are presented in Sect. 4. Some technical points are reported in Appendices.

2 A Spectral Approach to Survival Probability

2.1 Matrix Representation

We consider independent particles diffusing inside a bounded domain Ω with a smooth reflecting boundary $\partial\Omega$. At time $t = 0$, the particles are distributed with a given initial density $\rho(\mathbf{r}_0)$. For a given function $B(\mathbf{r})$, a random variable

$$\phi_t = \int_0^t ds\ B(X_s)$$

is associated to a random trajectory X_s of the reflected Brownian motion in Ω. Intuitively, the function $B(\mathbf{r})$ can be thought of as a distribution of "markers" for distinguishing different points and regions of the confining domain. When the diffusing particle passes through these regions, the random variable ϕ_t accumulates the corresponding "marks". In other words, different parts of the trajectory are weighted according to the function $B(\mathbf{r})$, encoding thus the

whole stochastic process. For example, if the bulk contains traps, reactive regions, absorbing sinks or relaxing impurities, $B(\mathbf{r})$ can represent the distribution of their trapping, reaction, absorption or relaxation rates, respectively, while ϕ_t is the cumulant factor penalizing the trajectories that pass through these regions. When $B(\mathbf{r})$ is an applied magnetic field, ϕ_t is the total dephasing of the nuclei in a pulsed-gradient spin-echo NMR experiment [47].

We recall that the probability distribution of the random variable ϕ_t can be found in two steps [50]. The first step is based on the classical Kac formula relating the expectation $\mathbb{E}\{e^{-h\phi_t}\}$ to the solution of a diffusion equation with bulk relaxation [51, 52]. This expectation includes the average of the functional $e^{-h\phi_t}$ over all the random trajectories $\{X_s\}_{0\le s\le t}$ of the reflected Brownian motion between the starting point $\mathbf{r}_0$ at time 0 and the arrival point $\mathbf{r}$ at time t, as well as the average over all $\mathbf{r}_0$ and $\mathbf{r}$ with given initial density $\rho(\mathbf{r}_0)$ and weighting function $\tilde{\rho}(\mathbf{r}_0)$ respectively; in this case, Kac formula reads as [50]

$$\mathbb{E}\{e^{-h\phi_t}\} = \int_\Omega d\mathbf{r}\, c(\mathbf{r}, t)\tilde{\rho}(\mathbf{r}), \tag{1}$$

where $c(\mathbf{r}, t)$ obeys the equation

$$\frac{\partial c(\mathbf{r}, t)}{\partial t} - D\Delta c(\mathbf{r}, t) + hB(\mathbf{r})c(\mathbf{r}, t) = 0, \tag{2}$$

with the initial condition $c(\mathbf{r}_0, t = 0) = \rho(\mathbf{r}_0)$, and $\Delta = \frac{\partial^2}{\partial x_1^2} + \cdots + \frac{\partial^2}{\partial x_d^2}$ is the Laplace operator in d dimensions. The reflected character of Brownian motion is represented by Neumann boundary condition, when the normal derivative $\partial/\partial n$ at the boundary vanishes: $\partial c(\mathbf{r}, t)/\partial n = 0$ on $\partial\Omega$. If $B(\mathbf{r})$ is the distribution of bulk sinks (or their absorption rates), $c(\mathbf{r}, t)$ can be interpreted as the probability density for a Brownian particle, started according to the initial density $\rho(\mathbf{r}_0)$, to arrive in an infinitesimal vicinity of the point $\mathbf{r}$ at time t, without being trapped, reacted, absorbed or relaxed during its motion. The weighting function $\tilde{\rho}(\mathbf{r})$ allows one to delimit the region of interest inside the confining domain. Since $c(\mathbf{r}, t)$ is weighted by $\tilde{\rho}(\mathbf{r})$ in (1), only those Brownian trajectories that arrived into the "pickup" regions at time t do contribute to the expectation in (1).

At the second step, one uses the Laplace operator eigenfunctions $u_m(\mathbf{r})$ $(m = 0, 1, 2, \ldots)$ that satisfy

$$D\Delta u_m(\mathbf{r}) + \lambda_m u_m(\mathbf{r}) = 0 \quad (\mathbf{r} \in \Omega),$$
$$\frac{\partial u_m(\mathbf{r})}{\partial n} = 0 \quad (\mathbf{r} \in \partial\Omega),$$

λ_m being the Laplace operator eigenvalues. Since the eigenfunctions $u_m(\mathbf{r})$ form a complete orthonormal basis, the solution $c(\mathbf{r}, t)$ of (2) can be expanded as

$$c(\mathbf{r}, t) = \sum_{m'} c_{m'}(t)u_{m'}(\mathbf{r}).$$

Substitution of this expansion in (2), multiplication by $u_m^*(\mathbf{r})$, and integration over Ω yield a set of ordinary differential equations for the unknown coefficients $c_m(t)$,

$$\frac{\partial c_m(t)}{\partial t} + \sum_{m'} (\Lambda_{m,m'} + h\mathcal{B}_{m,m'})c_{m'}(t) = 0,$$

where the infinite-dimensional matrices $\mathcal{B}$ and Λ are

$$\mathcal{B}_{m,m'} = \int_\Omega d\mathbf{r}\, u_m^*(\mathbf{r}) B(\mathbf{r}) u_{m'}(\mathbf{r}),$$
$$\Lambda_{m,m'} = \delta_{m,m'}\lambda_m.$$

Thinking of $c_m(t)$ as components of an infinite-dimensional vector $C(t)$, one easily finds the solution of the above matrix equation. The expectation $\mathbb{E}\{e^{-h\phi_t}\}$ can thus be written in a form of a scalar product:

$$S_h(t) = \mathbb{E}\{e^{-h\phi_t}\} = (U e^{-(\Lambda+h\mathcal{B})t}\tilde{U}), \tag{3}$$

where the infinite-dimensional vectors U and $\tilde{U}$ represent the projections of the initial density $\rho(\mathbf{r})$ and the weighting function $\tilde{\rho}(\mathbf{r})$ onto the eigenfunctions $u_m(\mathbf{r})$:

$$\begin{aligned} U_m &= \int_\Omega d\mathbf{r}\, u_m^*(\mathbf{r})\rho(\mathbf{r}), \\ \tilde{U}_m &= \int_\Omega d\mathbf{r}\, u_m(\mathbf{r})\tilde{\rho}(\mathbf{r}). \end{aligned} \tag{4}$$

The matrix $e^{-(h\mathcal{B}+\Lambda)t}$ can be thought of as a kind of evolution operator acting on the initial state $\rho(\mathbf{r})$ (represented by the vector U). The resulting density $c(\mathbf{r},t)$ at time t is then weighted by the weighting function $\tilde{\rho}(\mathbf{r})$ (represented by the vector $\tilde{U}$). It is important to note that the matrices $\mathcal{B}$ and Λ do not commute.

For a positive h, the expectation $\mathbb{E}\{e^{-h\phi_t}\}$ can be interpreted as the Laplace transform of the probability density $p_t(\varphi)$ of ϕ_t,

$$\mathbb{E}\{e^{-h\phi_t}\} = \int_0^\infty d\varphi\; e^{-h\varphi} p_t(\varphi),$$

allowing one, at least formally, to find the latter by the inverse Laplace transform. Thus, the properties of the expectation $\mathbb{E}\{e^{-h\phi_t}\}$ provides a complete probabilistic description of the random variable ϕ_t.

2.2 Multi-exponential Decay

Since the matrix $\Lambda + h\mathcal{B}$ is symmetric, all its eigenvalues γ_m^h are real and can be ordered as $\gamma_0^h \le \gamma_1^h \le \gamma_2^h \le \cdots$. The corresponding eigenvectors form an orthogonal matrix V such that

$$\Lambda + h\mathcal{B} = V \begin{pmatrix} \gamma_0^h & 0 & 0 & 0 & \cdots \\ 0 & \gamma_1^h & 0 & 0 & \cdots \\ 0 & 0 & \gamma_2^h & 0 & \cdots \\ 0 & 0 & 0 & \gamma_3^h & \cdots \end{pmatrix} V^T. \tag{5}$$

The substitution of (5) into (3) yields

$$S_h(t) = \sum_{m=0}^\infty A_m^h e^{-\gamma_m^h t}, \tag{6}$$

where

$$A_m^h = (UV)_m (V^T\tilde{U})_m. \tag{7}$$

The eigenvalues γ_m^h define the "lifetimes", $1/\gamma_m^h$, of the eigenmodes, while A_m^h set their relative contributions to $S_h(t)$. This multi-exponential decay is a generic feature for diffusive processes in bounded reactive media, whatever the spatial heterogeneity $B(\mathbf{r})$ is. For instance, Brownstein and Tarr derived similar relation for surface relaxation in NMR experiments [8].

In the long-time regime, the only significant contribution comes from the smallest eigenvalue λ_0^h which can therefore be interpreted as the overall reaction rate k. In what follows, the focus will be on this spectral characteristics.

2.3 Residence and Survival Times

How long does a diffusing particle reside in a given subset A of a confining domain Ω up to time t? This so-called residence (or occupation) time, ϕ_t, can be computed through the spectral approach by setting $B(\mathbf{r}) = \mathbb{I}_A(\mathbf{r})$, where $\mathbb{I}_A(\mathbf{r})$ is the indicator function of the set $A : \mathbb{I}_A(\mathbf{r}) = 1$ for $\mathbf{r} \in A$, and 0 otherwise [47, 48, 50, 53]. This function can be thought of as a "counter" which is turned on whenever the diffusing particle resides in A. The inverse Laplace transform of the survival probability $S_h(t)$ with respect to h gives, at least formally, the probability density of the residence time ϕ_t (here t is a fixed parameter).

In addition, the survival probability allows one to retrieve the first passage time τ at the reactive region A. In fact, if a particle hits A during the time interval $[0, t]$, then $\phi_t > 0$, while $\phi_t = 0$ otherwise. So, the limit of $\mathbb{E}\{e^{-h\phi_t}\}$ as $h \to \infty$ is the probability that a random trajectory X_s does not hit the set A up to time t:

$$S_\infty(t) = \lim_{h\to\infty} \mathbb{E}\{e^{-h\phi_t}\}.$$

This is the survival probability in a medium containing infinitely reactive regions, in which particles react or relax at the first hit, i.e., $S_\infty(t) = \mathbb{P}\{\tau > t\}$. The time derivative, $-dS_\infty(t)/dt$, is then the probability density of the first passage time τ.

In analogy, the survival probability $S_h(t)$ can be interpreted as the cumulative distribution function $\mathbb{P}\{\tau_h > t\}$ where τ_h is the survival time, i.e., a random moment, at which a particle reacts in a medium with finite reactivity h or, equivalently, up to which the particle survives. Since a particle may hit a partially reactive boundary many times without being reacted, the random moment τ_h at which reaction occurs, can also be termed as "the last passage time" [54]. The probability density of τ_h is $-\partial S_h(t)/\partial t$.

In summary, the spectral representation (6) allows one to study various time statistics of the diffusive process in heterogeneous reactive media. In Sect. 4, we analyze the long-time behavior of the survival probability for surface reaction ($A \subset \partial\Omega$) and bulk reaction ($A \subset \Omega$).

3 Numerical Implementation

In this section, we describe an implementation of the spectral approach for computing the survival probability $S_h(t)$ on the unit interval or the unit disk containing a given reactive region A. The matrix Λ is formed by the Laplace operator eigenvalues which are known explicitly for these confining domains, while the computation of the matrix $\mathcal{B}$ relies on the integration of two explicitly known eigenfunctions over A:

$$\mathcal{B}_{m,m'} = \int_A d\mathbf{r}\, u_m(\mathbf{r}) u_{m'}(\mathbf{r}). \tag{8}$$

In what follows, we recall the form of the Laplace operator eigenbasis, describe the main steps of the numerical algorithm, and discuss accuracy and improvements.

3.1 Eigenbasis in 1D and 2D

For the unit interval $\Omega = [0, 1]$ with reflecting endpoints, the eigenvalues and eigenfunctions of the Laplace operator are

$$\lambda_m = \pi^2 m^2, \quad u_m(x) = \varepsilon_m \cos(\pi m x) \quad (m = 0, 1, 2, \ldots),$$

with the normalization constants $\varepsilon_m = \sqrt{2}$ for $m > 0$, and $\varepsilon_0 = 1$.

Since the eigenvalues are known explicitly and integrals with cosine functions can be computed analytically, both matrices Λ and $\mathcal{B}$ have explicit forms so that the survival probability in the unit interval with any reactive region A can easily be found. For example, if A is the boundary of Ω, $A = \{0, 1\}$, the matrix $\mathcal{B}$ is

$$\mathcal{B}_{m,m'} = \varepsilon_m \varepsilon_{m'} [1 + (-1)^{m-m'}].$$

Simple computations for the unit interval allow one to analyze in depth the performances of the spectral approach.

For the unit disk $\Omega = \{\mathbf{r} \in \mathbb{R}^2 : |\mathbf{r}| < 1\}$, the eigenfunctions of the Laplace operator with Neumann boundary condition are [47, 48, 55–57]

$$\begin{aligned} u_{nk0}(r, \varphi) &= \frac{\sqrt{2}}{\sqrt{\pi}} \frac{\beta_{nk}}{J_n(\alpha_{nk})} J_n(\alpha_{nk} r) \cos(n\varphi) \\ u_{nk1}(r, \varphi) &= \frac{\sqrt{2}}{\sqrt{\pi}} \frac{\beta_{nk}}{J_n(\alpha_{nk})} J_n(\alpha_{nk} r) \sin(n\varphi) \end{aligned} \quad (n > 0), \tag{9}$$

$$u_{0k0}(r, \varphi) = \frac{1}{\sqrt{\pi}} \frac{\beta_{0k}}{J_0(\alpha_{0k})} J_0(\alpha_{0k} r) \quad (n = 0).$$

For each $n \geq 0$, α_{nk} $(k = 0, 1, 2, \ldots)$ denote all the positive roots of the equation:

$$J_n'(z) = 0, \tag{10}$$

where $J_n(z)$ is the Bessel function of the first kind, and prime denotes the derivative. The eigenvalues are $\lambda_{nk} = \alpha_{nk}^2$, while the normalization constants β_{nk} are defined as [55]

$$\beta_{nk} = \sqrt{\frac{\lambda_{nk}}{\lambda_{nk} - n^2}}.$$

The eigenvalues, eigenfunctions and other spectral quantities are conveniently enumerated by double or triple index, nk or nkl, instead of a single index m. This enumeration is also used for the related vectors and matrices, e.g., $\mathcal{B}_{nkl,n'k'l'}$ is the element of the matrix $\mathcal{B}$ (not a tensor!) that corresponds to the eigenfunctions $u_{nkl}(\mathbf{r})$ and $u_{n'k'l'}(\mathbf{r})$ (cf. (8)).

3.2 Algorithm

For numerical implementation, the eigenvalues λ_{nk} are sorted in an ascending order to truncate the infinite-dimensional matrices $\mathcal{B}$ and Λ. The position of the eigenmode in such a sequence can be used as its single index m.

The numerical algorithm consists of the following steps:

1. For a chosen truncation size N, to determine the first N Laplace operator eigenvalues λ_{nk} in the unit disk. For this purpose, one finds the first positive roots of (10) with different values of n by the bisection method. Since the eigenvalues λ_{nk} depend only on the confining domain, this step has to be performed only once, and the stored values of λ_{nk} can then be used in following computations.
2. For a given reactive region A, to compute the truncated matrix $\mathcal{B}$ of size $N \times N$. Except for certain specific cases, for which the integral in (8) can be found explicitly by using the properties of Bessel functions [56, 58], a numerical integration is required. For this purpose, the region A is conveniently discretized and integrals are approximated by finite sums. This step is time-consuming and is a major source of numerical inaccuracy.
3. For a given reactivity h, to compute the eigenvalues γ_m^h and eigenvectors V_m of the matrix $\Lambda + h\mathcal{B}$. This step is the most time-consuming when the size N of the matrix $\Lambda + h\mathcal{B}$ is large.
4. For a chosen initial density $\rho(\mathbf{r})$ and weighting function $\tilde{\rho}(\mathbf{r})$, to find the truncated vectors U and $\tilde{U}$ according to (4). When the starting and arrival points are irrelevant, the functions $\rho(\mathbf{r})$ and $\tilde{\rho}(\mathbf{r})$ are considered to be uniform, in which case $U_m = \tilde{U}_m = \delta_{m,0}$. In other cases, a numerical integration may be required, as in the step 2.
5. To get the amplitudes A_m^h from (7).
6. If necessary, to extrapolate γ_m^h and A_m^h to the limit of N going to infinity (see below).

As a result, the survival probability $S_h(t)$ is obtained in its explicit spectral form (6).

The computation involves two approximations: numerical integration in (8) and truncation of the matrices Λ and $\mathcal{B}$. The first approximation is classical, and its error is relatively easy to control. The second approximation is more subtle, and its accuracy strongly depends on the reactive region A. In order to illustrate this point, we consider A to be a small region. In this case, slowly varying eigenfunctions (i.e., with small eigenvalues) are almost constant on A so that the corresponding elements of the matrix $\mathcal{B}$ are: $\mathcal{B}_{m,m'} \approx u_m(\mathbf{r}_A)u_{m'}(\mathbf{r}_A)S_A$, S_A being the surface area of A, and $\mathbf{r}_A$ a point in A. It means that slowly varying eigenfunctions cannot distinguish the shape of a small region A. In order to reveal small geometrical features of A, highly oscillating eigenfunctions (i.e., with large eigenvalues) have to be included. In this sense, the truncation size N determines how accurate the spatial resolution of a spectral decomposition is. The choice of an appropriate value for N is therefore strongly dependent on the reactive region A. Since the computational time for finding eigenvalues and eigenvectors of a matrix of size $N \times N$ grows as $O(N^3)$, this may be a limiting factor for using the spectral approach, especially for small reactive regions. In this specific case, perturbative techniques are preferred [27, 28, 30–34].

3.3 Rotation-invariant Reactive Regions

The above numerical limitation can be overcome when the reaction rate distribution $B(\mathbf{r})$ is rotation-invariant (i.e., $B(r, \varphi)$ is independent of φ). In this case, the Laplace operator eigenvalues can be grouped in such a way that the matrix $\mathcal{B}$ gets a block structure. In fact, one has

$$\mathcal{B}_{nk0,n'k'0} = \mathcal{B}_{nk1,n'k'1} = 2\delta_{n,n'} \frac{\beta_{nk}\beta_{nk'}}{J_n(\alpha_{nk})J_n(\alpha_{nk'})} \times \int_0^1 dr\, r J_n(\alpha_{nk}r) J_n(\alpha_{nk'}r) B(r),$$

$$\mathcal{B}_{nk0,n'k'1} = \mathcal{B}_{nk1,n'k'0} = 0.$$

Instead of previously used ascending order, let us now order the first N eigenvalues as

$$\underbrace{\lambda_{00}, \lambda_{01}, \ldots, \lambda_{0k_0}}_{\text{block } 0}, \underbrace{\lambda_{10}, \lambda_{11}, \ldots, \lambda_{1k_1}}_{\text{block } 1}, \ \ldots \ \underbrace{\lambda_{n-1,0}, \lambda_{n-1,1}, \cdots, \lambda_{n-1,k_{n-1}}}_{\text{block } n-1}, \underbrace{\lambda_{n0}}_{\text{block } n},$$

where the indices $k_0, k_1, \ldots$ are chosen such that $\lambda_{j,k_j+1} > \lambda_{\max}$ $(j = 0, 1, \ldots)$, and the index n is such that $\lambda_{n+1,0} > \lambda_{\max}$ (here $\lambda_{\max}$ is the maximal eigenvalue among the first N eigenvalues). It is worth stressing that the eigenvalues λ_{nk} with $n > 0$ are twice degenerate and they should appear twice in the above sequence. The matrix $\mathcal{B}$ is then decomposed into block matrices $\mathcal{B}^j$:

$$\mathcal{B} = \begin{pmatrix} \mathcal{B}^0 & & & & 0 \\ & \mathcal{B}^1 & & & \\ & & \mathcal{B}^2 & & \\ & & & \cdots & \\ 0 & & & & \mathcal{B}^n \end{pmatrix},$$

where $\mathcal{B}^j_{k,k'} = \mathcal{B}_{jk0,jk'0}$ $(j = 0, \ldots, n)$. Since Λ is a diagonal matrix, it can also be written in a form of blocks. Consequently, the diagonalization of the matrix $\Lambda + h\mathcal{B}$ is reduced to *separate* diagonalizations of the (much) smaller matrices $\Lambda^j + h\mathcal{B}^j$. This gives a tremendous gain in computational time that allowed us to increase the value of N up to 10^5.

When studying the long-time regime, only the smallest eigenvalue γ_0^h is needed, and it turns out to be the smallest eigenvalue of the first block matrix $\Lambda^0 + h\mathcal{B}^0$. Although this statement is not yet proved rigorously, there are strong numerical evidences for its correctness.

3.4 Convergence and Accuracy

In the remainder of this section, we analyze the accuracy of the spectral approach for computing γ_0^h. For this purpose, we consider several examples for which the theoretical value of γ_0^h is known. Since large h is expected to be more problematic for computing the eigenvalues of the matrix $\Lambda + h\mathcal{B}$ (because the "perturbation" $h\mathcal{B}$ is large), the value $h = 10^8$ is taken as a proxy for the limit of h going to infinity. This limit corresponds to a perfectly reactive/absorbing/relaxing medium, in which particles are "killed" at the first encounter with A.

Example 1 $\Omega = (0, 1)$ (the unit interval), $A = \{0, 1\}$ (two endpoints). Figure 1 shows the smallest eigenvalue $\gamma^h_{0,N}$ of the matrix $\Lambda + h\mathcal{B}$ truncated to size $N \times N$ as a function of N ranging from 500 to 2500. One gets

$$\gamma^h_{0,N} \approx 9.8696 + \frac{8.0301}{N},$$

where the limiting value 9.8696 is very close to the theoretical value $\gamma_0^\infty = \pi^2 \approx 9.8696\ldots$ (the smallest eigenvalue of the Laplace operator on the unit interval with Dirichlet boundary conditions).

Example 2 $\Omega = (0, 1)$ (the unit interval), $A = [0.2, 0.8]$ (subinterval). Figure 2 shows $\gamma^h_{0,N}$ as a function of N ranging from 400 to 1000, which can be fitted as

$$\gamma^h_{0,N} \approx 61.593 + \frac{92.92}{N}.$$

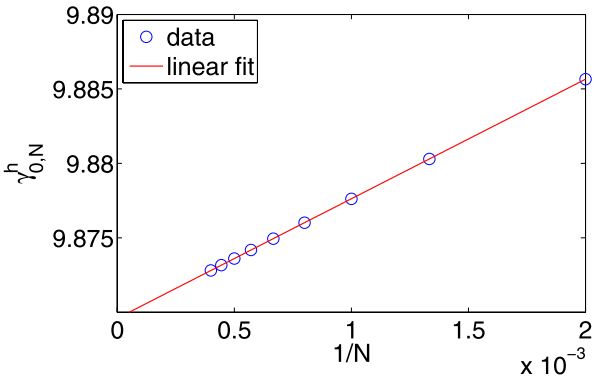

Fig. 1 (Color online) The smallest eigenvalue $\gamma^h_{0,N}$ of the truncated matrix $\Lambda + h\mathcal{B}$ (of size $N \times N$) for $\Omega = (0, 1)$, $A = \{0, 1\}$, $h = 10^8$. The error is almost linear with $1/N$

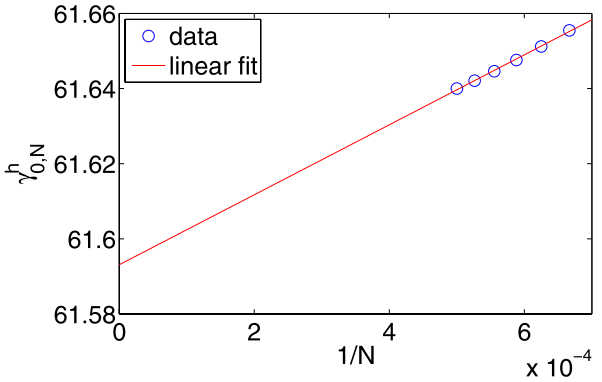

Fig. 2 (Color online) The smallest eigenvalue $\gamma^h_{0,N}$ of the truncated matrix $\Lambda + h\mathcal{B}$ (of size $N \times N$) for $\Omega = (0, 1)$, $A = [0.2, 0.8]$, $h = 10^8$. The error is approximately linear with $1/N$

The limiting value 61.593 is close to the theoretical value $\gamma_0^\infty = \pi^2/(2 \cdot 0.2)^2 \approx 61.685\ldots$ (the smallest eigenvalue of the Laplace operator on the interval $[0, 0.2]$ with the reflecting endpoint 0 and the absorbing endpoint 0.2).

In general, when A is a compact subset of the unit interval, we proved that the error of computation is in the order of $1/N$ (the proof will be published elsewhere):

$$\gamma^h_{0,N} \approx \gamma^h_0 + \frac{const}{N}. \tag{11}$$

At first thought, a slow convergence to the limit may be considered as a significant limitation of the spectral approach. At the same time, the knowledge of the convergence rate allows one to extrapolate numerical values to the limit. In other words, one can compute $\gamma^h_{0,N}$ (or other spectral characteristics) for different N and then fit them by a linear function of $1/N$. It is worth noting that such supplementary steps do not almost increase the computational time. In fact, once the matrix $\Lambda + h\mathcal{B}$ of the largest available size N is constructed, finding the eigenvalues of its smaller submatrices is much faster than finding the eigenvalues of the matrix $\Lambda + h\mathcal{B}$ itself.

Example 3 $\Omega = \{\mathbf{r} \in \mathbb{R}^2 : |\mathbf{r}| < 1\}$ (the unit disk), $A = \partial\Omega$ (its boundary). Figure 3 shows $\gamma^h_{0,N}$ as a function of N ranging from 5000 to 17000 which can be fitted as

$$\gamma^h_{0,N} \approx 5.7829 + \frac{3.732}{\sqrt{N}}.$$

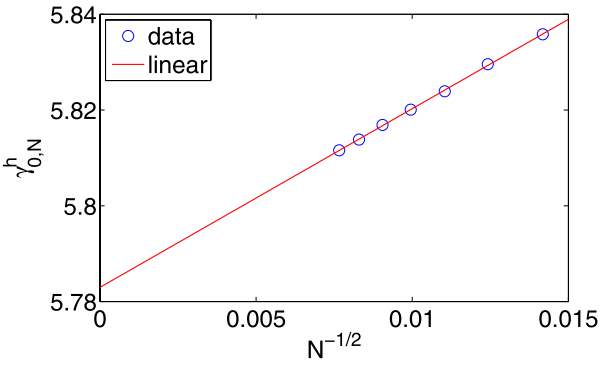

Fig. 3 (Color online) The smallest eigenvalue $\gamma^h_{0,N}$ of the truncated matrix $\Lambda + h\mathcal{B}$ (of size $N \times N$) for the unit disk, when A is the unit circle, and $h = 10^8$. The error is almost linear with $1/\sqrt{N}$

The limiting value 5.7829 is very close to the theoretical value $\gamma_0^\infty = 5.7832\ldots$ (the square of the first positive root α_{00} of the equation $J_0(z) = 0$, which is the smallest eigenvalue of the Laplace operator on the unit disk with Dirichlet boundary condition).

Example 4 $\Omega = \{\mathbf{r} \in \mathbb{R}^2 : |\mathbf{r}| < 1\}$ (the unit disk), $A = \{\mathbf{r} \in \mathbb{R}^2 : |\mathbf{r}| < r_0\}$ (smaller disk of radius $r_0 = 0.5$ shown on Fig. 5a). Figure 4 shows the value $\gamma^h_{0,N}$ as a function of N ranging from 10^4 to $1.9 \cdot 10^4$ which can be fitted as

$$\gamma^h_{0,N} \approx 7.345 + \frac{81.016}{\sqrt{N}}.$$

The limiting value 7.345 is very close to the theoretical value $7.3474\ldots$ (the square of the first positive root of (13) from Appendix B with $r_0 = 0.5$, which is the smallest eigenvalue of the Laplace operator on the circular layer with inner absorbing circle and outer reflecting circle).

In general, the error of computation is expected to be in the order of $\frac{1}{\sqrt{N}}$:

$$\gamma^h_{0,N} \approx \gamma^h_0 + \frac{const}{\sqrt{N}}.$$

A slower convergence for two-dimensional domains is expected from Weyl's asymptotic law for the eigenvalues: $\lambda_N \sim N^{2/d}$ [59]. In fact, the error of computation is related to the largest eigenvalue λ_N in the truncated matrix Λ so that (11) implies the error to be in the order of $\lambda_N^{-1/2}$ in the one-dimensional case. Assuming the same behavior of the error in higher dimensions, one gets the error in the order of $N^{-1/d}$, as confirmed by numerical results. Although the convergence is even slower in two dimensions than in one dimension, an extrapolation can still be used to get accurate results (e.g., see Examples 3 and 4).

A significant improvement can be achieved for rotation-invariant functions $B(\mathbf{r})$. As shown in Sect. 3.3, the matrix $\Lambda + h\mathcal{B}$ has a block structure, and the computation is reduced to the diagonalization of each block. We checked numerically that the smallest eigenvalue of a block matrix of size $n \times n$ behaves as

$$\gamma^h_{0,n} \approx \gamma^h_0 + \frac{const}{n},$$

as in the one-dimensional case. The extrapolation is also useful. In summary, the computation for the rotation-invariant case runs faster and uses a smaller number of eigenvalues to estimate more accurately the value of γ^h_0 than in the general case.

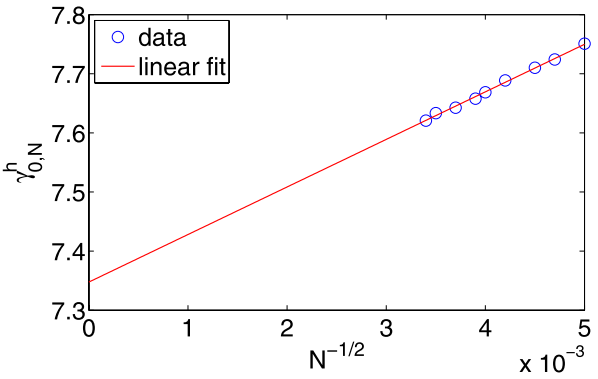

Fig. 4 (Color online) The smallest eigenvalue $\gamma^h_{0,N}$ of the truncated matrix $A + h\mathcal{B}$ (of size $N \times N$) for the unit disk, when A is a smaller disk of radius $r_0 = 0.5$, and $h = 10^8$. The error is approximately linear with $1/\sqrt{N}$

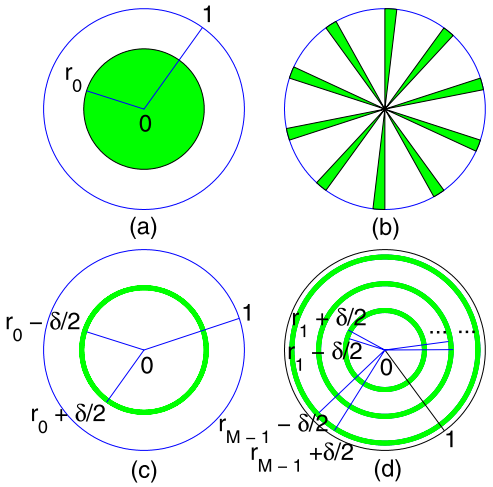

Fig. 5 (Color online) Several shapes of the reactive region A inside the unit disk. (**a**) A smaller disk of radius r_0 centered at the origin; (**b**) the union of M identical angular sectors of angle β, with the total area $S_A = M\beta/2$ fixed to be $\pi/4$. (**c**) A circular annulus of the inner and outer radii $r_0 - \delta/2$ and $r_0 + \delta/2$, centered at the origin; (**d**) the union of $M - 1$ annuli centered at the origin, with the inner and outer radii $r_i - \delta/2$ and $r_i + \delta/2$, and $r_i = i/M$, $i = 1, \ldots, M - 1$

4 Numerical Results

4.1 Surface Reaction on the Unit Circle

As we already mentioned, reactive regions may lie either in the bulk, or on the boundary of a confining domain. In the latter case, although the boundary is formally reflecting, particles can eventually react when hitting the boundary. Traditionally, partially reflecting-absorbing surfaces are modeled through Robin (also known as Fourier, third, radiation, mixed, etc.) boundary condition [60–63]:

$$\frac{\partial u^h_m(\mathbf{r})}{\partial n} + h u^h_m(\mathbf{r}) = 0 \quad (\mathbf{r} \in \partial\Omega),$$

with a positive constant h. In the presented spectral approach, the reflecting character of the surface is incorporated through the Laplace operator eigenfunctions with Neumann boundary condition, while the absorbing counter-part is introduced through the matrix $\mathcal{B}$. As pointed out in [48], such a separation of reflection and absorption "mechanisms" has several advantages. First, one can easily introduce heterogeneous reaction rate on the boundary (as

illustrated below). Second, the eigenfunctions $u_m^h(\mathbf{r})$ with Robin boundary condition depend on h, and have to be recalculated for each value of h. In turn, h appears as a constant in the matrix $\Lambda + h\mathcal{B}$ so that there is no need for reconstructing the matrices Λ and $\mathcal{B}$.

A numerical validation of the above implementation of the surface reaction mechanism was illustrated on Figs. 1 and 3. In these examples, the Laplace operator eigenfunctions with Neumann boundary condition (reflecting surface) were used to compute γ_0^∞, that is the smallest eigenvalue of the Laplace operator with Dirichlet boundary condition (absorbing boundary). The accuracy of this computation was remarkably good.

In order to illustrate the use of heterogeneous reaction rate on the surface, we consider two cases. First, we take A to be an arc of length 2ε. When ε is small, this is so-called narrow escape problem which was thoroughly studied by Singer et al. [27, 28]. In particular, they found the exact formula for the mean exit time from the unit disk. As discussed in Sect. 2.3, the survival probability allows one to investigate first passage times and other time statistics of Brownian motion in reactive media. In Appendix C, we express the mean exit time in terms of the spectral characteristics γ_m^h and A_m^h and compare the numerical results to the exact formula.

Second, we choose A to be the union of M identical arcs of the unit circle:

$$A = \left\{ \mathbf{r} \in \mathbb{R}^2 : r_1 = \cos\varphi,\ r_2 = \sin\varphi,\ \varphi \in \bigcup_{k=1}^{M} \left(\frac{2\pi k}{M}, \frac{2\pi k + L}{M} \right) \right\}.$$

The total length L of these arcs is fixed. The smallest eigenvalue γ_0^h for $h = 10^8$ is extrapolated to the limit $N \to \infty$ and plotted on Fig. 6 as a function of M for $L = 2\pi/5$. One can see that γ_0^h rapidly approaches the limit $5.7829\ldots$ as M increases. The same behavior was observed for other choices of the total length L (ranging between 0 and 2π). It means that a partly reactive boundary, in which many small reactive grains are equidistributed, has almost the same overall reaction rate as a fully reactive boundary, i.e., a small amount of catalytic grains (here, small length L) works as efficiently as a large amount of catalytic grains. In other words, if the catalytic grains are equidistributed over the surface, its performance is independent of the amount of catalytic grains (the length L).

This result, which sounds paradoxical at first thought, has a simple probabilistic explanation. When Brownian motion first hits the boundary at some point $\mathbf{r}$, it is killed immediately if $\mathbf{r} \in A$, or reflected otherwise. In the latter case, Brownian motion continues the diffusive exploration of the bulk near the boundary. If the boundary is smooth, reflected Brownian motion returns to the boundary after the first hit infinitely many times during an infinitely

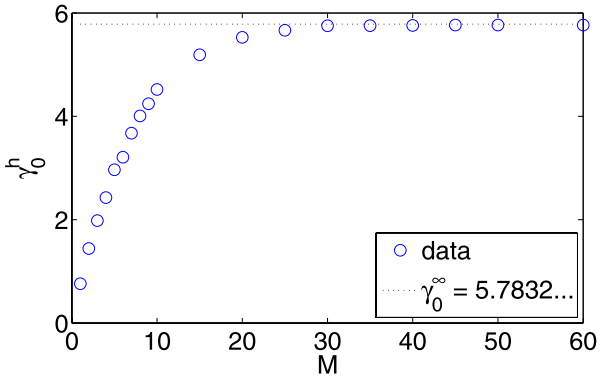

Fig. 6 (Color online) The extrapolated smallest eigenvalue γ_0^h for the unit disk, when A is composed of M identical arcs of the unit circle. The total length L is kept to be $2\pi/5$ for different M, and $h = 10^8$. When M increases, the eigenvalue γ_0^h rapidly approaches the limit $5.7832\ldots$ which corresponds to a perfectly reactive circle (cf. Fig. 3)

short time period. During these multiple reflections, Brownian motion explores the vicinity of the first hitting point. In the limit of $M \to \infty$, a small absorbing arc is always located near this point, and Brownian motion finds it with probability 1. In other words, after the first arrival onto the boundary, reflected Brownian motion finds the reactive region within infinitely short time when $M \to \infty$. As a consequence, there is almost no difference between reaction at the first hit (on a perfectly reactive boundary) and reaction after many infinitely short reflections (on a boundary with many equidistributed reactive regions). Another (analytical) proof of this result is given in Appendix A.

Although the above result is justified from a mathematical point of view, it still remains puzzling from a physical point of view. It is worth recalling that the classical model of Brownian diffusion towards perfectly reactive regions has limitations. In fact, the above mathematical consideration assumed that

- Brownian diffusion describes the motion of particles at any length scale that is obviously not true (diffusion is an accurate model only at length scales that are much longer than the mean free path of particles);
- the length of individual arcs can be arbitrarily small (resulting from the limit $M \to \infty$ with the fixed total length L) which is not applicable (there is always a minimal cut-off, e.g., the size of molecules);
- the reactivity is infinite which may also be questionable.

Since diffusion equation and the underlying spectral description are broadly applied to describe migrations and reactions of molecules in chemistry and biology, one should keep in mind potential limitations and pitfalls of this model. In particular, the use of a finite reactivity may be a way to overcome the above paradoxes (see below).

4.2 Infinite Reactivity in the Bulk

In analogy to Sect. 4.1, we consider A to be the union of M identical sectors of the unit disk (Fig. 5b), with the total surface area S_A to be fixed $\pi/4$. For numerical computations, $h = 10^8$ is chosen as a proxy for the infinite limit. Table 1 shows the values of γ_0^h, which tend to $S_A h/\pi$ for increasing M (see Appendix A).

If the reactivity h was infinite, one would expect $\gamma_0^\infty \to \infty$ as $M \to \infty$, independently of the total surface area S_A. Although the probabilistic argument from Sect. 4.1 formally explains this seemingly paradoxical behavior, this mathematical result is not applicable to real physical systems because of the limitations evoked in Sect. 4.1. In what follows, we focus on the case of a finite reactivity which seems to be more relevant for practical situations.

4.3 Finite Reactivity in the Bulk

When the reactivity h is finite, the amount of reactive grains can be naturally characterized by hS_A, S_A being the total area of the reactive region. Fixing hS_A, one may wonder how the

Table 1 The extrapolated smallest eigenvalue γ_0^h for the union of M identical sectors of the unit disk (Fig. 5b), with the total surface area $S_A = \pi/4$, and $h = 10^8$. When M increases, γ_0^h approaches the limit $h/4 = 2.5 \cdot 10^7$

M	1	5	10	15	20	30	35	50
γ_0^h	2.43	30.26	126.18	626.38	807.15	$1.50 \cdot 10^5$	$2.49 \cdot 10^6$	$2.49 \cdot 10^7$

reaction performance of the medium depends on the reactivity h and the shape of the reactive region. For instance, what is the shape of the most reactive medium? For the computations of this section, we fix $hS_A = \pi$ and analyze the smallest eigenvalue γ_0^h. We focus on the unit disk as the confining domain.

In the trivial case $A = \Omega$, (8) yields $\mathcal{B}_{m,m'} = \delta_{m,m'}$ due to the orthogonality of the eigenfunctions. The matrix $\mathcal{B}_\Omega$ is just the identity matrix, and γ_0^h is equal to h.

Example 1 $A = \{\mathbf{r} \in \mathbb{R}^2 \,:\, |\mathbf{r}| < r_0\}$ (the disk of radius r_0). The condition $hS_A = \pi$ implies $h = 1/r_0^2$ which varies from 1 to infinity as r_0 goes from 1 to 0. The behavior of γ_0^h is shown on Fig. 7.

When r_0 is close to 1, the reactive region is nearly the whole disk so that $\gamma_0^h \approx h \approx 1$. In the opposite limit of r_0 going to 0, the values γ_0^h approach 0, as one may expect for a shrinking reactive region. However, the decay is logarithmically slow, as in the case of a perfectly reactive region ($h = \infty$). In fact, the probability for Brownian motion to find (and then react immediately on) a small disk vanishes logarithmically with its radius r_0 in two dimensions. The asymptotic behavior of γ_0^∞ as $r_0 \to 0$ is given in Appendix B. On the other hand, for a reactive region with fixed h, a perturbative theory yields

$$\gamma_0^h \approx \lambda_0 + h\mathcal{B}_{0,0} = hr_0^2 \quad (r_0 \to 0)$$

that is a much faster decay. The example shown on Fig. 7 is a somewhat intermediate situation, in which the condition $hS_A = \pi$ makes the first-order perturbative term hr_0^2 to be constant. In this case, the whole perturbative series has to be computed for a fixed r_0, and the resulting sum turns out to decay logarithmically as $r_0 \to 0$.

Since γ_0^h decays logarithmically, even a very small reactive region yields a significant reaction rate γ_0^h as shown on Fig. 7 (although the values of γ_0^h seem to approach a positive constant, it is a visual deception).

Example 2 $A = \{\mathbf{r} \in \mathbb{R}^2 \,:\, r_0 - \delta/2 < |\mathbf{r}| < r_0 + \delta/2\}$. Another interesting example is a circular annulus with the inner and outer radii $r_0 - \delta/2$ and $r_0 + \delta/2$ (Fig. 5c). When δ is small, the matrix $\mathcal{B}$ can be approximated as

$$\mathcal{B}_{nkl,n'k'l'} = \int_{r_0-\delta/2}^{r_0+\delta/2} dr\, r \int_0^{2\pi} d\varphi u_{nkl}(r,\varphi) u_{n'k'l'}(r,\varphi) \approx r_0 \delta \mathcal{B}^{(0,r_0)}_{nkl,n'k'l'},$$

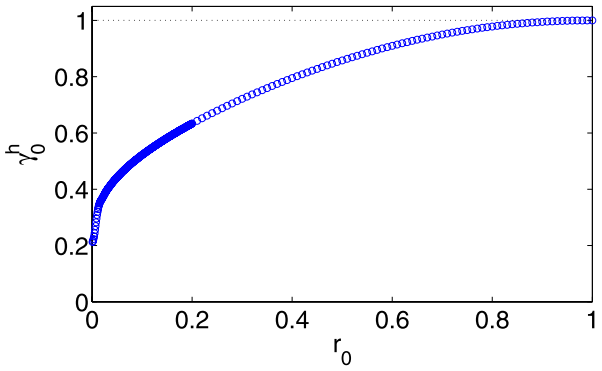

Fig. 7 (Color online) The extrapolated smallest eigenvalue γ_0^h as a function of the radius r_0 of the reactive region (the disk) shown on Fig. 5a, with $hS_A = \pi$

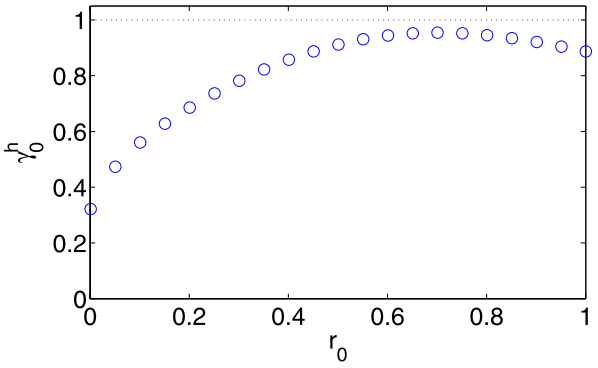

Fig. 8 (Color online) The extrapolated smallest eigenvalue γ_0^h as a function of the radius r_0 of the reactive region (the annulus of width δ) shown on Fig. 5c, with $hS_A = \pi$ and $\delta \to 0$

where

$$\mathcal{B}^{(0,r_0)}_{nkl,n'k'l'} = \int_0^{2\pi} d\varphi u_{nkl}(r_0,\varphi) u_{n'k'l'}(r_0,\varphi)$$

is the matrix $\mathcal{B}$ for a perfectly reactive circle of radius r_0 (centered at the origin). Since the condition $hS_A = \pi$ implies $hr_0\delta = 1/2$, the matrix $\Lambda + h\mathcal{B}$ becomes

$$\Lambda + h\mathcal{B} \approx \Lambda + hr_0\delta\mathcal{B}^{(0,r_0)} = \Lambda + \frac{1}{2}\mathcal{B}^{(0,r_0)}.$$

The behavior of γ_0^h is shown on Fig. 8. Interestingly, there is an optimal radius $r_0 \approx 0.7$ for which a thin circular annulus has the highest reaction rate γ_0^h. The latter is slightly below 1 that is the reaction rate for a uniformly filled unit disk (under the condition of fixed $hS_A = \pi$). This is an example of geometry optimization for reactive media (see below).

Example 3 Multiple equidistant annuli shown on Fig. 5d.

Next, we consider A be to the union of M thin annuli shown on Fig. 5d, each annulus having the width δ. The total area S_A is $\pi\delta(M-1)$, implying $h\delta(M-1) = 1$. When $\delta \to 0$, the matrix $\Lambda + h\mathcal{B}$ converges to

$$\Lambda + h\mathcal{B} \approx \Lambda + h\delta \sum_{i=1}^{M-1} r_i \, \mathcal{B}^{(0,r_i)} = \Lambda + \frac{1}{M(M-1)} \sum_{i=1}^{M-1} i \, \mathcal{B}^{(0,r_i)}.$$

As shown on Fig. 9, the value of γ_0^h tends to 1 when the number M of annuli increases.

Our numerical examples suggest that a uniform filling of a medium with reactive grains of finite reactivity h provides the highest overall reaction rate γ_0^h. This seems to be the optimal geometry of the reactive region under the constraint of fixed hS_A. A theoretical argument supporting this suggestion is presented in Appendix D, while a rigorous proof is still missing. However, such a uniform filling is not available in many practical situations (e.g., when multiple processes have to be maintained in parallel, like in the case of a living cell). In this case, one may wonder whether it is possible to fill the medium heterogeneously nearly as good as uniformly, and what is the optimal shape of the reactive region (perhaps, under some additional constraints).

Two examples of this section illustrate these issues. Figure 8 shows that there is an optimal radius for a single thin circular annulus (i.e., under specific geometrical constraint),

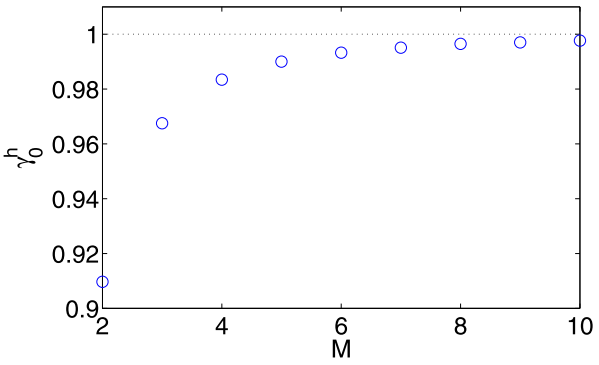

Fig. 9 (Color online) The extrapolated smallest eigenvalue γ_0^h as a function of the number M of annuli shown on Fig. 5d, with $hS_A = \pi$ and $\delta \to 0$

while Fig. 9 confirms that the performance of several thin circular annuli is nearly as good as the best one (for uniform filling). These "toy" models can be considered as the first steps towards geometrical design and engineering of optimal catalysts and diffusive exchangers.

Conclusion

We presented a spectral approach for computing the survival probability of reflected Brownian motion in reactive media. For arbitrary spatial distribution $B(\mathbf{r})$ of trapping, reaction or relaxation rate, a multi-exponential representation of the survival probability was derived. Its amplitudes A_m^h and characteristic times $1/\gamma_m^h$ were expressed through the spectral properties of the two infinite-dimensional matrices Λ and $\mathcal{B}$ which represent the Laplace operator and the distribution $B(\mathbf{r})$ in the Laplace operator eigenbasis on a chosen confining domain. The advantage of such a representation is that the geometrical complexity of the problem (i.e., the shape of reactive regions) is incorporated through the matrix $\mathcal{B}$, independently of the Laplace operator eigenbasis. In other words, computation of the eigenfunctions, which is often the most time-consuming step, has to be performed only once for a given confining domain. Moreover, in many cases, the shape of the confining domain is irrelevant, and simple confining domains such as a disk or a sphere can be used. In these cases, the Laplace operator eigenfunctions and eigenvalues are known explicitly that significantly simplifies computations. For this reason, we considered the unit disk as a confining domain.

From a numerical point of view, the computational performance of the spectral approach may be inferior to other numerical techniques. It is not surprising because the conventional techniques (such as Monte Carlo simulations or finite difference or finite element methods) search for a single solution of a diffusive problem with a given set of physical parameters. On the contrary, the use of eigenfunctions allows one to find (or, at least, to formally express) all the solutions at once and to analyze the structure of these solutions and their dependence on physical parameters. This much more detailed information comes at the cost of more time-consuming computations. In the general case of any spatial distribution of reactive regions, the accuracy of the algorithm is in the order of $N^{-1/d}$, while the computational time for finding eigenvalues of an $N \times N$ matrix grows as $O(N^3)$, where N is the number of the eigenfunctions used, and d is the space dimension. Nonetheless, an extrapolation to the limit $N \to \infty$ allows one to get reasonably accurate results. In addition, we showed that significant improvements in computational time and accuracy can be achieved for rotation-invariant reactive regions. More importantly, a multi-exponential representation (6) of the

survival probability provides a much deeper insight onto diffusive processes in reactive media than other numerical techniques. The spectral approach computes separately a large number of terms in (6), while other techniques approximates the whole sum. As a consequence, an accurate determination of rapidly decaying terms (with high eigenvalues) is unfeasible by conventional methods.

Using the spectral approach, we studied the role of the geometrical structure of reactive regions and its influence on the overall reaction rate γ_0^h in the long-time regime. For this purpose, we computed the survival probability in several model reactive media and showed that the shape and spatial arrangement of reactive regions could significantly affect γ_0^h. When the reactivity h was infinite, the confining domain could be filled with numerous reactive regions of arbitrarily small total surface area to make the overall reaction rate arbitrarily high. Although this seemingly paradoxical result was justified from a mathematical point of view, it could not have practical applications because of the physical limitations of diffusion model. For the case of finite reactivity h, we discussed the optimization of the geometrical shape of reactive regions under the constraint of having fixed total reactivity (i.e., fixed product hS_A). A uniform filling with $A = \Omega$ appeared as the optimal solution yielding the highest reaction rate. In turn, heterogeneity tends to reduce the reaction rate. However, when such a uniform filling is not possible (or undesired), one can still arrange the reactive regions heterogeneously in a way to get the reaction rate almost as good as the optimal one. This is an interesting perspective for designing the geometrical shapes of efficient catalysts or diffusive exchangers.

Acknowledgement The work has been partly supported by the ANR grant "DYOPTRI".

Appendix A: Equidistributed Arcs and Sectors

When a reactive region A lies on the boundary of the unit disk, finding the elements of the matrix $\mathcal{B}$ is reduced to computation of integrals over the angular coordinate φ that can be performed analytically. For instance, if the reactive region is composed of M identical arcs of angle β which are equidistributed over the circle (Sect. 4.1), the truncated matrix $\mathcal{B}$ of size $N \times N$ takes a simple form for $M > 2N + 1$

$$\mathcal{B}_{nkl,n'k'l'} = [2\delta_{n,n'}\delta_{l,l'}(1 - \delta_{l,1}\delta_{l',1}\delta_{n,0}\delta_{n',0})\beta_{nk}\beta_{n'k'}]\frac{M\beta}{2\pi} \tag{12}$$

(when $M \leq 2N + 1$, a more complicated explicit formula can also be derived). When M increases in such a way that the total length $L = M\beta$ of the arcs is kept constant, the truncated matrix $\mathcal{B}$ is

$$\mathcal{B} = \frac{L}{2\pi}\mathcal{B}^{(\partial\Omega)},$$

where $\mathcal{B}^{(\partial\Omega)}$ denotes the matrix in the large brackets of (12) and corresponds to the matrix $\mathcal{B}$ for the reactive region $A = \partial\Omega$ (the whole boundary of the unit disk). As a consequence, the survival probability for a large number M of arcs (partly reactive boundary) turns out to approach the survival probability for the whole circle (fully reactive boundary) when $h = \infty$.

Similarly, when A is the union of M identical angular sectors of angle β which are equidistributed in the unit disk (Fig. 5b), the truncated matrix $\mathcal{B}$ gets a simple form

$$\mathcal{B} = \frac{S_A}{\pi}I,$$

where the identity matrix I is the matrix $\mathcal{B}$ for the unit disk.

Appendix B: Analytical Results for Reactive Disks

We consider the survival probability for infinitely reactive region ($h = \infty$) in the shape of a disk of radius r_0 centered at the origin (Fig. 5a). This problem is equivalent to diffusion in a circular layer $\Omega_1 = \{\mathbf{r} \in \mathbb{R}^2 : r_0 < |r| < 1\}$ with the absorbing inner circle of radius r_0 and the reflecting outer circle of radius 1. The smallest eigenvalue α^2 of the Laplace operator in this layer is determined by the first positive root α of the following equation [53, 56, 57]

$$J_0(\alpha r_0) Y_0'(\alpha) - Y_0(\alpha r_0) J_0'(\alpha) = 0, \tag{13}$$

where $J_0(z)$ and $Y_0(z)$ are the Bessel functions of the first and second kind, respectively. Solving numerically this equation, one can find the theoretical value $\gamma_0^\infty = \alpha^2$ for any r_0 between 0 and 1. In the limit of r_0 going to 1, the following asymptotic behavior can be derived

$$\gamma_0^\infty \approx \frac{\pi^2}{4(1-r_0)^2} \quad (r_0 \to 1). \tag{14}$$

In the opposite limit of r_0 going to 0, the asymptotic behavior of Bessel functions allows one to reduce (13) to

$$\gamma_0^\infty \approx \frac{2}{\ln(a/r_0)} + \frac{\ln(\ln(a/r_0)/2)}{(\ln(a/r_0))^2} \quad (r_0 \to 0), \tag{15}$$

where $a = 2e^{-\gamma}$ and $\gamma = 0.5772157\ldots$ is the Euler-Mascheroni constant. Although γ_0^∞ approaches 0 as $r_0 \to 0$, the decay is logarithmically slow so that even very small reactive regions may yield significant reaction rates, as shown on Fig. 7. Note that the logarithmically slow decay is the specific feature of the two-dimensional case.

It is worth noting that the limits $r_0 \to 1$ and $h \to \infty$ cannot be exchanged. In fact, for numerical computations, one always uses a large but finite value of h (e.g., $h = 10^8$). In this case, the asymptotic behavior of γ_0^h as $r_0 \to 1$ is different from (14). Denoting $\varepsilon = 1 - r_0$, we have

$$\mathcal{B} = \mathcal{B}^{(\Omega)} - \mathcal{B}^{(\Omega_1)} \approx I - \varepsilon \mathcal{B}^{(\partial\Omega)},$$

where $\mathcal{B}^{(\partial\Omega)}$ corresponds to $B(\mathbf{r}) = \mathbb{I}_{\partial\Omega}(\mathbf{r})$. The matrix $\Lambda + h\mathcal{B}$ can then be approximated as

$$\Lambda + h\mathcal{B} \approx (\Lambda + hI) - h\varepsilon \mathcal{B}^{(\partial\Omega)}.$$

For a finite h, the last term appears as a correction to the first one so that

$$\gamma_0^h \approx h(1 - O(\varepsilon)) \quad (\varepsilon \to 0).$$

Appendix C: Narrow Escape Problem

Singer and co-workers dealt with the exit problem from the unit disk with reflecting boundary, except for an absorbing arc of length 2ε [27, 28]. For Brownian motion $\mathbf{x}(t)$ started from the origin, the mean exit time is found to be

$$\mathbb{E}[\tau | \mathbf{x}(0) = (0,0)] = \frac{\sqrt{2}}{2\pi} \int_0^{\pi-\varepsilon} \frac{u \sin\frac{u}{2}}{\sqrt{\cos u + \cos\varepsilon}}\, du + \frac{1}{4}. \tag{16}$$

When the absorbing part shrinks to zero, this formula yields the following asymptotic behavior

$$\mathbb{E}[\tau\,|\mathbf{x}(0)=\mathbf{0}] = \log\frac{1}{\varepsilon} + \log 2 + \frac{1}{4} + O(\varepsilon).$$

These two analytical formulas can be used for checking spectral computations.

Starting from the origin is introduced into the spectral approach through the point-like initial density $\rho(\mathbf{r}_0) = \delta(\mathbf{r}_0)$, where $\delta(\mathbf{r}_0)$ is the Dirac distribution. The vector U becomes

$$U_{nkl} = \frac{\delta_{n,0}\delta_{l,0}}{J_n(\alpha_{nk})}, \quad n = 0, 1, \ldots,\ k = 0, 1, \ldots,\ l = 0, 1.$$

Since the weighting function $\tilde{\rho}(\mathbf{r})$ remains constant, the vector $\tilde{U}$ does not change:

$$\tilde{U}_{nkl} = \delta_{n,0}\delta_{k,0}\delta_{l,0}, \quad n = 0, 1, \ldots,\ k = 0, 1, \ldots,\ l = 0, 1.$$

Using (6), the mean exit time from the unit disk can be computed as

$$\mathbb{E}[\tau\,|\mathbf{x}(0)=(0,0)] = \sum_{m=0}^{\infty} \frac{A_m^{\infty}}{\gamma_m^{\infty}}. \tag{17}$$

Figure 10 helps to compare (16, 17) for the mean exit time as a function of ε. As we discussed in Sect. 3.3, the accuracy of the spectral approach decreases when ε is getting smaller. Since the spectral computation of the mean exit time includes both the truncation of the matrix $\Lambda + h\mathcal{B}$ and the truncation of the series in (17), the results are not as good as for the smallest eigenvalue γ_0^h. Nevertheless, an extrapolation helps to get reasonably accurate results even for small ε (up to 0.01).

A more direct comparison can be realized for the smallest eigenvalue γ_0^{∞} whose asymptotic behavior was derived by Ward and co-workers [32]. For a single arc of length 2ε, their asymptotic formula reads as

$$\gamma_0^{\infty} \approx -\frac{1}{\ln(\varepsilon/2)} - \frac{1}{8[\ln(\varepsilon/2)]^2} + O([\ln(\varepsilon/2)]^{-3}). \tag{18}$$

Since the expansion parameter here is $\ln(\varepsilon/2)$ (and not ε itself), this formula is only applicable for small ε. On Fig. 11, we compare the asymptotic result (18) to the γ_0^{∞} computed

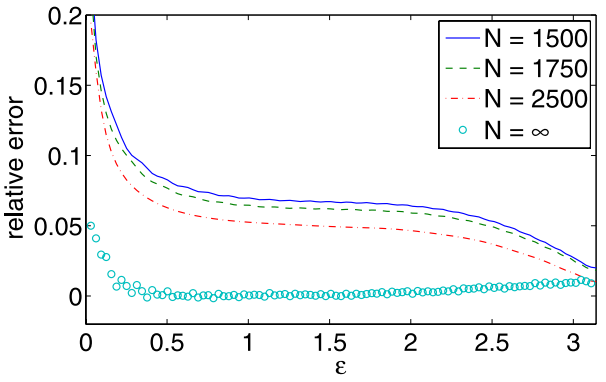

Fig. 10 (Color online) The relative error between the exact formula (16) and the truncated spectral representation (17) for the mean exit time from the unit disk whose boundary is reflecting but for an absorbing arc of length 2ε

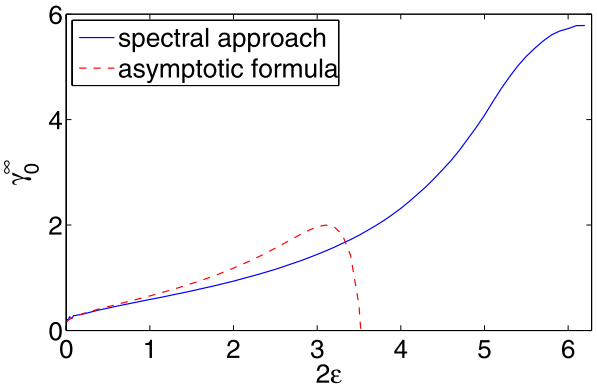

Fig. 11 (Color online) The smallest eigenvalue γ_0^∞ for the unit disk when the reactive region is an arc of length 2ε (with $h = 10^8$). When 2ε goes to 2π (the whole circle), γ_0^∞ approaches the theoretical value $5.7829\ldots$, as expected. The asymptotic formula (18) is accurate for small ε but inapplicable for large ε

by the spectral approach. As expected, two curves are close to each other for small ε. It is worth stressing again that, for smaller ε, the spectral computation requires larger matrices and takes longer time, while the asymptotic formula is getting more accurate. On the contrary, when 2ε exceeds 1, the asymptotic formula becomes less and less accurate, and it finally diverges at $\varepsilon = 2$.

In summary, when the reactive regions are very small, perturbative techniques are preferred [27, 28, 30–34]. In turn, the spectral approach is more appropriate for extended reactive regions, for which perturbative techniques become useless. These two approaches are complementary to each other.

Appendix D: Optimal Reactive Region

Numerical evidences (Figs. 7, 9) suggest that a uniform filling of a confining domain provides the highest overall reaction rate γ_0^h under the condition that the total amount of reactive grains is fixed. We propose a theoretical argument in favor of this statement, although a rigorous proof is still missing. This argument relies on a perturbation theory applied to the matrix $\Lambda + h\mathcal{B}$. In the limit of small h, the smallest eigenvalue γ_0^h can be written as a perturbation series in powers of h. Keeping the terms up to the second order in h, we get

$$\gamma_0^h \approx \lambda_0 + h\mathcal{B}_{0,0} - h^2 \sum_{m>0} \frac{\mathcal{B}_{0,m}\mathcal{B}_{m,0}}{\lambda_m - \lambda_0} = \frac{h}{S}\int_\Omega d\mathbf{r}\; B(\mathbf{r}) - h^2 \sum_{m>0} \frac{\mathcal{B}_{0,m}^2}{\lambda_m}$$

(since $\lambda_0 = 0$). The first term is the total amount of reactive grains (which may have spatially heterogeneous reactivities incorporated via $B(\mathbf{r})$). In our numerical examples, when $B(\mathbf{r}) = \mathbb{I}_A(\mathbf{r})$, the first term was simply hS_A/S. Since this term is supposed to be fixed, the influence of $B(\mathbf{r})$ on γ_0^h is represented through the second term. For a uniform filling with $A = \Omega$, $\mathcal{B}_{m,m'} = \delta_{m,m'}$ so that the second term is zero. Since $\lambda_m > 0$, the uniform filling is indeed optimal for getting the highest γ_0^h:

$$\gamma_0^h \le \gamma_{0,\mathrm{uni}}^h = h.$$

Further analysis is required for a rigorous proof of this result.

References

1. Weiss, G.H.: Aspects and Applications of the Random Walk. North-Holland, Amsterdam (1994)
2. Redner, S.: A Guide to First-Passage Processes. Cambridge University Press, Cambridge (2001)
3. Hughes, B.D.: Random Walks and Random Environments. Clarendon, Oxford (1995)
4. Weiss, G.H.: Overview of theoretical models for reaction rates. J. Stat. Phys. **42**, 3 (1986)
5. Coppens, M.-O.: The effect of fractal surface roughness on diffusion and reaction in porous catalysts: from fundamentals to practical application. Catalysis Today **53**, 225–243 (1999)
6. Zwanzig, R., Szabo, A.: Time dependent rate of diffusion-influenced ligand binding to receptors on cell surfaces. Biophys. J. **60**, 671–678 (1991)
7. Holcman, D., Marchewka, A., Schuss, Z.: Survival probability of diffusion with trapping in cellular neurobiology. Phys. Rev. E **72**, 031910 (2005)
8. Brownstein, K.R., Tarr, C.E.: Importance of classical diffusion in NMR studies of water in biological cells. Phys. Rev. A **19**, 2446–2453 (1979)
9. Smoluchowski, M.V.: Phys. Z. **17**, 557 (1916)
10. Balagurov, B.Ya., Vaks, V.G.: Random walks of a particle on lattices with traps. J. Exp. Theor. Phys. **38**, 968 (1974)
11. Grassberger, P., Procaccia, I.: The long time properties of diffusion in a medium with static traps. J. Chem. Phys. **77**, 6281–6284 (1982)
12. Kayser, R.F., Hubbard, J.B.: Diffusion in a medium with a random distribution of static traps. Phys. Rev. Lett. **51**, 79 (1983)
13. Kayser, R.F., Hubbard, J.B.: Reaction diffusion in a medium containing a random distribution of nonoverlapping traps. J. Chem. Phys. **80**, 1127 (1984)
14. Lee, S.B., Kim, I.C., Miller, C.A., Torquato, S.: Random-walk simulation of diffusion-controlled processes among static traps. Phys. Rev. B **39**, 11833 (1989)
15. Torquato, S., Kim, I.C.: Efficient simulation technique to compute effective properties of heterogeneous media. Appl. Phys. Lett. **55**, 1847 (1989)
16. Miller, C.A., Torquato, S.: Diffusion-controlled reactions among spherical traps: effect of polydispersity in trap size. Phys. Rev. B **40**, 7101 (1989)
17. Miller, C.A., Kim, I.C., Torquato, S.: Trapping and flow among random arrays of oriented spheroidal inclusions. J. Chem. Phys. **94**, 5592 (1991)
18. Kansal, A.R., Torquato, S.: Prediction of trapping rates in mixtures of partially absorbing spheres. J. Chem. Phys. **116**, 10589 (2002)
19. Richards, P.M.: Diffusion to finite-size traps. Phys. Rev. Lett. **56**, 1838 (1986)
20. Richards, P.M.: Diffusion to nonoverlapping or spatially correlated traps. Phys. Rev. B **35**, 248 (1987)
21. Richards, P.M., Torquato, S.: Upper and lower bounds for the rate of diffusion-controlled reactions. J. Chem. Phys. **87**, 4612 (1987)
22. Rubinstein, J., Torquato, S.: Diffusion-controlled reactions: mathematical formulation, variational principles, and rigorous bounds. J. Chem. Phys. **88**, 6372 (1988)
23. Torquato, S., Avellaneda, M.: Diffusion and reaction in heterogeneous media: pore-size distribution, relaxation times, and mean survival time. J. Chem. Phys. **95**, 6477 (1991)
24. Torquato, S.: Diffusion and reaction among traps: some theoretical and simulation results. J. Stat. Phys. **65**, 1173 (1991)
25. Torquato, S., Yeong, C.L.Y.: Universal scaling for diffusion-controlled reactions among traps. J. Chem. Phys. **106**, 8814 (1997)
26. Riley, M.R., Muzzio, F.J., Buettner, H.M., Reyes, S.C.: The effect of structure on diffusion and reaction in immobilized cell systems. Chem. Eng. Sci. **50**, 3357 (1995)
27. Singer, A., Schuss, Z., Holcman, D., Eisenberg, R.S.: Narrow escape. Part I. J. Stat. Phys. **122**, 437 (2006)
28. Singer, A., Schuss, Z., Holcman, D.: Narrow escape. Part II: the circular disk. J. Stat. Phys. **122**, 465 (2006)
29. Bénichou, O., Voituriez, R.: Narrow-escape time problem: time needed for a particle to exit a confining domain through a small window. Phys. Rev. Lett. **100**, 168105 (2008)
30. Kolokolnikov, T., Titcombe, M.S., Ward, M.J.: Optimizing the fundamental Neumann eigenvalue for the Laplacian in a domain with small traps. Eur. J. Appl. Math. **16**, 161 (2005)
31. Ward, M.J.: Asymptotic methods for reaction-diffusion systems: past and present. Bull. Math. Biol. **68**, 1151 (2006)
32. Pillay, S., Ward, M.J., Peirce, A., Kolokolnikov, T.: An asymptotic analysis of the mean first passage time for narrow escape problems: part I. Two-dimensional domains. SIAM Multiscale Model. Simul. **8**, 803–835 (2010)

33. Cheviakov, A.F., Ward, M.J., Straube, R.: An asymptotic analysis of the mean first passage time for narrow escape problems: part II. The sphere. SIAM Multiscale Model. Simul. **8**, 836–870 (2010)
34. Cheviakov, A., Ward, M.J.: Optimizing the principal eigenvalue of the Laplacian in a sphere with interior traps. Math. Comput. Model. (2010). doi:10.1016/j.mcm.2010.02.025
35. Ryu, S.: Effects of inhomogeneous partial absorption and the geometry of the boundary on population evolution of molecules diffusing in general porous media. Phys. Rev. E **80**, 026109 (2009)
36. Ryu, S., Johnson, D.L.: Aspects of diffusive-relaxation dynamics with a nonuniform, partially absorbing boundary in general porous media. Phys. Rev. Lett. **103**, 118701 (2009)
37. Condamin, S., Bénichou, O., Tejedor, V., Voituriez, R., Klafter, J.: First-passage time in complex scale-invariant media. Nature **450**, 77 (2007)
38. Condamin, S., Bénichou, O., Moreau, M.: First-passage times for random walks in bounded domains. Phys. Rev. Lett. **95**, 260601 (2005)
39. Condamin, S., Bénichou, O., Moreau, M.: First-exit times and residence times for discrete random walks on finite lattices. Phys. Rev. E **72**, 016127 (2005)
40. Condamin, S., Bénichou, O., Moreau, M.: Random walks and Brownian motion: a method of computation for first-passage times and related quantities in confined geometries. Phys. Rev. E **75**, 021111 (2007)
41. Condamin, S., Tejedor, V., Bénichou, O.: Occupation times of random walks in confined geometries: from random trap model to diffusion-limited reactions. Phys. Rev. E **76**, 050102R (2007)
42. Yuste, S.B., Oshanin, G., Lindenberg, K., Bénichou, O., Klafter, J.: Survival probability of a particle in a sea of mobile traps: a tale of tails. Phys. Rev. E **78**, 021105 (2008)
43. Levitz, P.E., Grebenkov, D.S., Zinsmeister, M., Kolwankar, K., Sapoval, B.: Brownian flights over a fractal nest and first passage statistics on irregular surfaces. Phys. Rev. Lett. **96**, 180601 (2006)
44. Callaghan, P.T.: A simple matrix formalism for spin echo analysis of restricted diffusion under generalized gradient waveforms. J. Magn. Reson. **129**, 74–84 (1997)
45. Barzykin, A.V.: Theory of spin echo in restricted geometries under a step-wise gradient pulse sequence. J. Magn. Reson. **139**, 342–353 (1999)
46. Axelrod, S., Sen, P.N.: Nuclear magnetic resonance spin echoes for restricted diffusion in an inhomogeneous field: methods and asymptotic regimes. J. Chem. Phys. **114**, 6878–6895 (2001)
47. Grebenkov, D.S.: NMR survey of reflected Brownian motion. Rev. Mod. Phys. **79**, 1077–1137 (2007)
48. Grebenkov, D.S.: Laplacian eigenfunctions in NMR I. A numerical tool. Concepts Magn. Reson. A **32**, 277–301 (2008)
49. Grebenkov, D.S.: Laplacian eigenfunctions in NMR II. Theorical advances. Concepts Magn. Reson. A **34**, 264–296 (2009)
50. Grebenkov, D.S.: Residence times and other functionals of reflected Brownian motion. Phys. Rev. E **76**, 041139 (2007)
51. Majumdar, S.N.: Brownian functionals in Physics and Computer Science. Curr. Sci. **89**, 2076 (2005)
52. Truman, A., Williams, D.: In: Pinsky, M.A. (ed.) Diffusion Processes and Related Problems in Analysis, vol. 1. Birkhauser, Basel (1990)
53. Grebenkov, D.S.: Analytical solution for restricted diffusion in circular and spherical layers under inhomogeneous magnetic fields. J. Chem. Phys. **128**, 134702 (2008)
54. Grebenkov, D.S.: Subdiffusion in a bounded domain with a partially absorbing/reflecting boundary. Phys. Rev. E **81**, 021128 (2010)
55. Grebenkov, D.S.: Multiple correlation function approach: rigorous results for simples geometries. Diffus. Fundam. **5**, 1 (2007)
56. Crank, J.: The Mathematics of Diffusion, 2nd edn. Clarendon, Oxford (1975)
57. Carslaw, H.S., Jaeger, J.C.: Conduction of Heat in Solids, 2nd edn. Clarendon, Oxford (1959)
58. Bowman, F.: Introduction to Bessel Functions, 1st edn. Dover, New York (1958)
59. Lapidus, M.: Fractal drum, inverse spectral problems for elliptic operators and a partial resolution of the Weyl-Berry conjecture. Trans. Am. Math. Soc. **325**, 465 (1991)
60. Collins, F.C., Kimball, G.E.: Diffusion-controlled reaction rates. J. Coll. Sci. **4**, 425–437 (1949)
61. Sapoval, B.: General formulation of Laplacian transfer across irregular surfaces. Phys. Rev. Lett. **73**, 3314–3317 (1994)
62. Grebenkov, D.S.: Partially reflected Brownian motion: a stochastic approach to transport phenomena. In: Velle, L.R. (ed.) Focus on Probability Theory, pp. 135–169. Nova Science Publishers, New York (2006)
63. Singer, A., Schuss, Z., Osipov, A., Holcman, D.: Partially reflected diffusion. SIAM J. Appl. Math. **68**, 844–868 (2008)